A DYNAMIC MODEL OF OPEN VESICLES IN FLUIDS *

ROLF J. RYHAM †, FREDRIC S. COHEN ‡, AND ROBERT EISENBERG §

Abstract. A hydrodynamic model of open vesicles in solution is presented to study the enlargement and shrinkage of a pore in biological lipid membrane. The vesicle is modeled by diffusive interfaces. Transport equations permitting consistent treatment of the pore and pore rim are introduced. Dynamic simulations implemented by the finite difference method show the evolution of a pore in stretched vesicles. Simulation results include direct visualization of the membrane shape, water motion, and dissipation of energy. Comparison is made with data obtained from microscopy experiments.

Key words. Phase field; Diffusive interface; Biological membranes; Pore dynamics; Finite difference methods.

subject classifications. MSC2010 74K15, 92B05, 92C05

1. Introduction. Biological membranes are composed of lipid molecules. Due to their hydrophobic and hydrophilic structure, the lipid molecules form two layers called the lipid bilayer. The bilayer separates regions of water and allows the membrane to act as a barrier. A vesicle is a small, fluid compartment formed by the bilayer. In biological processes such as exocytosis, the membrane of two vesicles merge to form a single bilayer. Pore formation is a similar topological change occurring in a single vesicle. The continuous vesicle is stretched so far that a pore forms in the membrane. The inner and outer water regions become connected. The vesicle becomes open.

The opening and closing of a pore plays an important role in biological systems because the pore allows movement between otherwise isolated compartments. In the past two decades, experimentalists have learned to create and measure pores by light microscopy. A well established mathematical model of this phenomenon was developed in [1]. The theory in [1] is widely used ([11, 13, 18]) to understand the evolution of a pore. For example, it has been adapted by [19] to the measure edge tension as a function of lipid composition. The theory of [1] imposes a geometry. The vesicle is spherical and the pore is round. A rate equation for the pore is coupled with a continuity equation for the water. Studying the simplified geometry has the advantage that the change in volume and radius of the pore are explicitly formulated in terms of rate equations. Parameters for the system of ordinary differential equations arising from the theory can be found that yield fits to the data.

In our model, we start with a pore and approximate the classical Helfrich energy ([10]) of an open vesicle using a diffusive interface, i.e. phase field, approximation. The novelty is that the shape of the vesicle is a variable and we calculate the line and surface forces from variational derivatives of the energy function. As a corollary, the exchange of energy from the membrane to the fluid, as well as the motion of the vesicle are self consistent. We emphasize that models which assume a particular shape can have quite different properties than reality. Imposing a shape is an artificial constraint and is equivalent to injecting energy into an otherwise isolated system.

*

†Fordham University, Department of Mathematics, 441 E. Fordham Road, Bronx, NY 10458, (rryham@fordham.edu).

‡Rush University Medical Center, Department of Molecular Biophysics and Physiology, 1750 W Harrison St, Chicago, IL 60612, (Fredric_Cohen@rush.edu).

§Rush University Medical Center, Department of Molecular Biophysics and Physiology, 1750 W Harrison St, Chicago, IL 60612, (beisenbe@rush.edu).

Communications in Mathematical Sciences (in the press)

In [26], Wang and Du developed a phase field model for multicomponent lipid membranes. Building on earlier work with Chun Liu [3], they studied the equilibrium shapes of vesicles with spatially varying membrane properties. Their numerical experiments are in strong qualitative agreement with known multicomponent membrane shapes. Their approximation is justified by asymptotic expansions. We have adapted the phase field functionals they used [26] to model a single pore in a vesicle.

The hydrodynamics of open vesicles present significant modeling challenges. Because an open vesicle exerts both line and surface forces, the model must capture hydrodynamic forces supported on one and two dimensional subsets. Because the pore is an opening in the membrane, the model must track a mathematical surface with boundary in a kinematically consistent way.

The diffusive interface method treats the membrane region as a thin, bulk material. The membrane, along with the aqueous solution, are viewed as a single fluid with a smoothly varying material property. Transporting the diffusive interface by the fluid changes the membrane's energy. In return, the diffusive interface imparts a force on the ambient fluid. The equations are discretized on a fixed computational domain. The boundary is usually the fluid far from the membrane. Since the diffusive interface is defined by a bulk field, one avoids tracking the membrane explicitly and simple boundary conditions may be employed.

We represent an open vesicle using two labeling functions. We define a function $\phi(x,t)$ by labeling the interior aqueous region, a diffuse interface containing the membrane, and outer aqueous region $-1,0$, and 1. Continuing, we define $\bar{\phi}(x,t)$ by labeling the part of the diffuse interface corresponding to water and the part corresponding to lipid by -1 and 1 respectively. $\phi(x,t)=0$ and $\bar{\phi}(x,t)=1$ implies x is a lipid and otherwise x is a water. The role of the labeling functions is illustrated in Figure 3.1.

The convergence of phase field models of bending energy was proved in [5] using asymptotic expansions. For the time dependent problem, [4] showed that a related hydrodynamic phase field model of a vesicle with bending energy was well posed. The theoretical justification for the convergence of phase field models to the classical continuum mechanical models of vesicle membranes has a long history beginning with the phase transition theory [2, 8, 15] leading up to today's higher order theories [16, 20]. There are also several other successful methods for modeling vesicle membranes in solution. In [14, 21, 23], immersed boundary and boundary integral methods capable of following large deformations of complex membranes over long time scales were proposed. To our knowledge, there are no three dimensional continuum simulations which describe open vesicles in solution.

The details of the diffusive interface energy are given in Section 2. The equations of motion are defined in Section 3. We used modified transport equations for $\phi(x,t)$ and $\bar{\phi}(x,t)$ that properly reflect the kinematics of the membrane and pore. These important details, as well as the derivation of the force, are discussed in Section 3. In Section 3.1, we use the scaling relationships of the energy to derive the nondimensional coefficients. Section 4 gives the simulation results visualizing the membrane shape, water motion, and dissipation of energy, as well as comparison with experimental results. Details of the discretization method are also found there.

Finally, we remark that biological membranes and vesicles are complicated materials involving several components and multiscale interactions. The problem we are considering here is highly simplified membrane model system. However, even the simplistic diffusive interface representation is able to capture the realistic dynamics. In order to be consistent with prior use of the terminology, we will refer to the fluid

compartment formed by the simple bilayer structure as a vesicle.

2. Diffusive Interface Functional. In this section, we introduce functionals used to approximate the classical continuum lipid membrane energy. Define the cutoff functions

$$\alpha(p)=\frac{1}{2}(\tanh(\xi p)+1),\quad \bar{\alpha}(p)=\operatorname{sech}^2(\xi p),\quad \xi>0.$$

The role of these cut-off functions will be explained below. Define the functionals

$$A=\frac{3}{2\sqrt{2}}\int_D \alpha(\bar{\phi})\left[\frac{\epsilon}{2}|\nabla\phi|^2+\frac{1}{\epsilon}F(\phi)\right]dx, \tag{2.1}$$

$$W=\frac{3}{4\sqrt{2}}\int_D \alpha(\bar{\phi})\epsilon\left[\Delta\phi-\frac{1}{\epsilon^2}F'(\phi)\right]^2 dx, \tag{2.2}$$

$$L=\frac{9}{8}\int_D\left(\frac{\epsilon}{2}|\nabla\phi|^2+\frac{1}{\epsilon}F(\phi)\right)\left(\frac{\epsilon}{2}|\nabla\bar{\phi}|^2+\frac{1}{\epsilon}F(\bar{\phi})\right)dx. \tag{2.3}$$

Here D is the three dimensional computational domain. The function $F(p)=\frac{1}{4}(p^2-1)^2$ is a double welled potential and ϵ is a small, positive parameter related to the thickness of the diffuse interface. The functional W approximates the mean curvature squared energy of the membrane surface, L approximates the circumference of the pore, and A approximates the membrane surface area. Define

$$E_p=bW+jL+s\frac{(A-A_{\mathrm{r}})^2}{2A_{\mathrm{r}}}+wA. \tag{2.4}$$

E_p approximates the Helfrich energy of the vesicle. The first term in (2.4) is the bending energy of the vesicle. It is the energetic contribution coming from the splay of the lipid molecules [10]. The second term is the edge energy[1]. When a pore is formed, lipid molecules reorient so that the hydrophilic head groups shield the membrane interior from water. The edge energy is proportional to pore circumference. The third term is a Hookean relationship accounting for the mechanical energy stored in excess area. It can also be used in a penalty formulation to enforce the constraint $A=A_{\mathrm{r}}$. Here, A_{r} is the area of the unstretched membrane. The membrane is inextensible when mechanical modulus s is large. The last term is surface energy. The coefficients b, j and w are the bending modulus, edge tension, and surface tension respectively.

In (2.1) and (2.2), the integrands are multiplied by $\alpha(\bar{\phi})$ so that only the component of the interface corresponding to membrane contributes to the total energy. In (2.3), the factors in the integrand approximate the area density of the two interfacial regions defined by ϕ and $\bar{\phi}$. The rim of the pore is located along the intersection of these regions. The product of the respective area densities in (2.3) yields a satisfactory approximation of the circumference of the pore.

To stabilize the method, we use the energy

$$E=E_p+\frac{m_1}{2}P^2+m_2\bar{W}, \tag{2.5}$$

where

$$\bar{W}=\frac{3}{4\sqrt{2}}\int_D \epsilon\left[\Delta\bar{\phi}-\frac{1}{\epsilon^2}F'(\bar{\phi})\right]^2 dx,\quad P=\int_D(\nabla\phi\cdot\nabla\bar{\phi})^2\,dx \tag{2.6}$$

[1] we distinguish between the terms line energy and edge energy. The former refers to the energy of the boundary of a domain within a multicomponent membrane.

are auxiliary functionals. Here m_1 is a penalty parameter for the constraint $P=0$. This constraint leads to orthogonal interfaces. The prefactor m_2 is a small, stabilizing parameter. In the sequel, E_ϕ and $E_{\bar\phi}$ denote the Euler-Lagrange derivative ([7]) of E with respect to ϕ and $\bar\phi$, respectively.

The following identities will be used to derive b, j, s, and w from known, physical constants. Let $D=\mathbb{R}^3$ and for $\lambda>0$, define ϕ_λ and $\bar\phi_\lambda$ by a dilation of space and define $\epsilon_\lambda=\lambda\epsilon$. Making the change of variables yields

$$A_\lambda=\lambda^2 A, \quad L_\lambda=\lambda L, \quad W_\lambda=W. \tag{2.7}$$

Here, the subscript λ is used to denote the functionals' dependence on ϕ_λ, $\bar\phi_\lambda$, and ϵ_λ.

3. Equations of Motion. To study the time course of the pore, we must evaluate the velocity of the membrane and aqueous solution. The velocity is determined by the equations of motion:

$$u_t+u\cdot\nabla u+\nabla p-\eta\Delta u=f, \tag{3.1}$$
$$\operatorname{div} u=0, \tag{3.2}$$
$$\phi_t+\alpha(\bar\phi)u\cdot\nabla\phi=-\gamma E_\phi, \tag{3.3}$$
$$\bar\phi_t+\bar\alpha(\phi)u\cdot\nabla\bar\phi=-\bar\gamma E_{\bar\phi}, \quad x\in D, \quad t>0. \tag{3.4}$$

Here, u is the velocity of a water molecule in the water region and the velocity of a lipid molecule in the membrane. p is the pressure. The force exerted by diffusive interface is given by the equation

$$f=\alpha(\bar\phi)E_\phi\nabla\phi+\bar\alpha(\phi)E_{\bar\phi}\nabla\bar\phi. \tag{3.5}$$

By equation (3.2), we are assuming that lipid and water are incompressible. We are assuming the vesicle and surrounding water have constant density. We are also assuming that the internal friction of the fluid, whether water, lipid, or at the water lipid interface, is Newtonian with a constant viscosity η. The viscosity of lipid membrane is typically greater than that of the solution. However, the membrane is very thin (a few nanometers) when compared to the overall geometry of the vesicle. Thus, the viscous dissipation in the membrane is much smaller than in the bulk aqueous medium. As the densities of water and lipid are comparable, we assume a constant density. Equations 3.3 and 3.4 are stabilized transport equations. The numbers γ and $\bar\gamma$ are small, positive stabilizing constants.

Equations 3.1 and 3.2 are complemented by the initial conditions $u(x,0)=u_0(x)$, $\operatorname{div}u_0=0$, $\phi(x,0)=\phi_0(x)$, and $\bar\phi(x,0)=\bar\phi_0(x)$. On the boundary, we assume a no-slip condition for the velocity and natural boundary conditions for the labeling functions:

$$u(x,t)=0, \quad \phi(x,t)=\bar\phi(x,t)=1, \quad \frac{\partial\phi}{\partial n}(x,t)=\frac{\partial\bar\phi}{\partial n}(x,t)=0, \quad x\in\partial D, t>0, \tag{3.6}$$

where $\frac{\partial}{\partial n}$ is the outward normal derivative on ∂D.

Cut-off functions are used to modulate the convective term in the transport equations. In equation 3.3, the convective term is multiplied by the cut-off function $\alpha(\bar\phi)$. As a result, ϕ is convected only where $\bar\phi$ takes positive values. In particular, the region of the diffusive interface inside the pore is not affected by the efflux of water. In equation 3.4, the label $\bar\phi$ is convected where ϕ takes values close to zero, that is, along the rim of the pore.

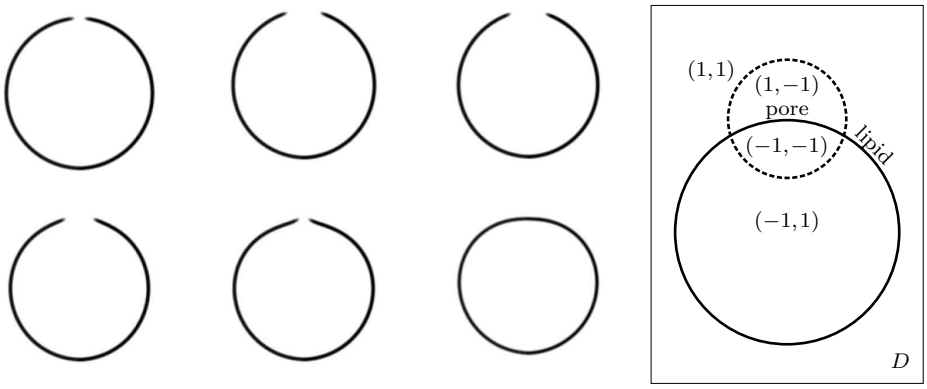

FIG. 3.1. *Left: cross sections of a vesicle with a hole as a function of time. Right: illustration of the pore defined by a pair of labeling functions* $(\phi(x),\bar{\phi}(x))$. *The diffusive interface* $\{\phi\approx 0\}$ *is drawn by a solid line and the diffusive interface* $\{\bar{\phi}\approx 0\}$ *is drawn by a dashed line.*

Equation 3.5 is derived using the principle of virtual work. The derivation is a modification of techniques developed in [6]. The modification deals mainly with defining a suitable variation of the domain based on the kinematic conditions described in the previous paragraph.

3.1. Nondimensional coefficients. We place a vesicle within a cylindrical aqueous medium of radius $\lambda\mu$m. We observe the vesicle over a characteristic time τs. The constants b,s,j and w are defined by

$$b=10^6\frac{b_0\tau^2}{\rho_0\lambda^5},\quad j=10^9\frac{j_0\tau^2}{\rho_0\lambda^4},\quad s=10^{12}\frac{s_0\tau^2}{\rho_0\lambda^3},\quad w=10^{12}\frac{w_0\tau^2}{\rho_0\lambda^3}. \tag{3.7}$$

Here b_0pNnm is the experimentally measured bending modulus, s_0pNnm^{-1} the stretching modulus, j_0pN the edge tension, w_0pNnm^{-1} the surface tension, and $\rho_0$gcm^{-3} the density of the solution. A realistic bending modulus is 80pNnm and realistic surface tension is 1pNnm^{-1}. As an illustration, a giant vesicle in experiment can typically be tens of microns in diameter and changes can appreciated over a time course seconds long. This scale yields a b on the order of 0.1 and w on the order of 10^7. The difference in magnitude of these constants suggests that bending, compared to surface tension, is irrelevant for the dynamics of large vesicles. To contrast, biological vesicles have diameters in the tens to hundreds of nanometers. Only in this regime and smaller are the constants b and w then comparable.

Let $\langle u,p,\phi,\bar{\phi}\rangle$ be a smooth solution of equations (3.1-3.6). Form the dot product equation (3.1) with u and integrate over D. Multiply (3.3) by E_ϕ and (3.4) by $E_{\bar{\phi}}$ and integrate over D. Integrating by parts using (3.2) and (3.6) then gives the energy law

$$\frac{d}{dt}\left(\int_D\frac{1}{2}|u|^2\,dx+E\right)+\int_D\eta|\nabla u|^2+\gamma|E_\phi|^2+\bar{\gamma}|E_{\bar{\phi}}|^2\,dx=0. \tag{3.8}$$

The details of a related calculation may be found in [4, 5]. Using (2.7), make the change of variables $\hat{t}=\tau t$s, $\hat{x}=\lambda x\mu$m, and $\hat{\epsilon}=\lambda\epsilon\mu$m. Matching the coefficients in (3.8)

with the dimensional coefficients b_0, s_0, j_0 and w_0 then yields (3.7). Readily apparent from this calculation is $\eta = 10^9 \eta_0 \tau (\rho_0 \lambda^2)^{-1}$ where η_0cP is the dynamic viscosity of the solution.

4. Simulation Results.

4.1. Discretization. To simulate the vesicle through equations (3.1-3.6), a spatial discretization by the finite difference method was developed. We simplified the problem to two dimensions by assuming a cylindrical geometry. Stretched vesicles with pores, as can be seen in the experimental images of [11], are axially symmetric. We assumed the vesicle was located in the rectangle $[0,1] \times [0,L]$. A fully implicit, backward Euler scheme was used in the time integration. For simplicity, the convective term was dropped from the Navier-Stokes equation. This assumption was justified by the fact the Reynolds number of flow in these biological systems is on the order of 10^{-2}.

A Picard iteration between the Stokes system and the parabolic sub-systems was used to solve for the velocity-pressure pair and the diffusive interface transport equations simultaneously. The Stokes system was solved using the preconditioned conjugate gradient routine found in [9], Algorithm 22.7.3. A mixed Picard-Newton's method was used to deal with the gradients of the discrete functional and the convective term. The linear systems were solved by SSOR preconditioned conjugate gradients. The stabilizing coefficients $\epsilon\gamma$ and $\epsilon\bar{\gamma}$ were small when compared to $(\Delta t^k)^{-1}$. The condition number of the Jacobian resulting from the discretization of stabilized transport equations was consequently not large. The algorithm was implemented in C.

For the spatial discretization, a uniform 128 by 256 grid was used. The diffuse interface thickness ϵ was chosen to be three times the mesh spacing Δx. This ensured that the interface was nicely resolved but remained thin when compared to the overall geometry of the vesicle. For the time integration, a uniform time step $\Delta t^k = 10^{-4}$ was used. The stability of the time integration, large fluid viscosity, stabilization parameters, and small step size ensured the monotonicity of energy. At each time the total energy was seen to be nonincreasing (Figure 4.1). The radius of the pore was calculated by averaging the r-coordinate of the overlap of the two diffusive interfaces. In the numerical experiments, the constraint and stability constants were $\gamma = \bar{\gamma} = 10^{-1}$, $m_1 = 10^3$, and $m_2 = 0.1$ respectively.

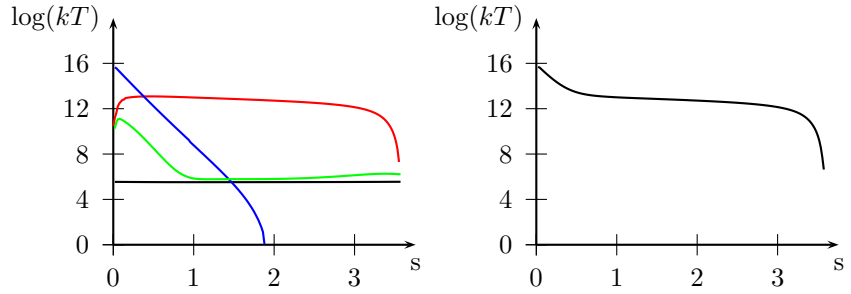

FIG. 4.1. *Energy as a function of time. Left: in the rapid opening stage, mechanical energy (blue) is converted into kinetic energy (green) and edge energy (red). Bending energy (black) is relatively constant. The kinetic energy increases briefly in rapid closing stage. Right: total energy is nonincreasing.*

Numerical tests were performed to check the sensitivity of the simulation with

respect to the grid size and with respect to the auxiliary parameters. In the first test, the simulation variables ϕ_h, $\bar{\phi}_h$, and u_h defined a fine, 128 by 256 grid were compared against the simulation variables ϕ_H, $\bar{\phi}_H$, and u_H defined on a course, 64 by 128 grid. In both cases the computational domain was $(0,1)\times(0,2)$ and all physical parameters and auxiliary parameters were held constant. In order to keep the diffusive interface thickness constant, ϵ was set to $6\Delta x$ on the fine grid and to $3\Delta x$ on the coarse grid. In Table 4.1, we see that the fine and course grid solutions differ by roughly 10% in the L^2-norm throughout the range of the simulation. The labeling functions differ in the L^∞-norm by roughly 20%, implying that the position of the diffusive interface differs by only a few grid points. In particular, the position of the vesicle and velocity are stable with respect to the grid size. To show that the dynamic is governed primarily by the diffusive interface energy, we also explored the dependence on the auxiliary constants. We compared the simulation when $\gamma=\bar{\gamma}=10^{-2}$, $m_1=10^3$, and $m_2=0.1$, the values used in the numerical experiments, against the simulation with the altered values $\gamma=\bar{\gamma}=2\cdot10^{-2}$, $m_1=0.5\cdot10^3$, and $m_2=0.2$. We have plotted the pore radius as a function of time for two sets of values for γ, $\bar{\gamma}$, m_1, and m_2 in Figure 4.2. The solid line corresponds to the values used in the numerical experiment while the dashed line corresponds to the altered values. We see that the overall dynamic is not greatly effected by doubling and halving the auxiliary values.

t	0.75s	1.25s	2.0s	2.75s	3.5s
$\|\phi_h-\phi_H\|_{L^2}$	0.097	0.085	0.081	0.079	0.077
$\|\bar{\phi}_h-\bar{\phi}_H\|_{L^2}$	0.012	0.018	0.021	0.021	0.021
$\|\phi_h-\phi_H\|_{L^\infty}$	0.229	0.281	0.280	0.275	0.269
$\|\bar{\phi}_h-\bar{\phi}_H\|_{L^\infty}$	0.205	0.244	0.246	0.246	0.246
$\|u_h-u_H\|_2/\|u_H\|_{L^2}$	0.126	0.070	0.061	0.070	0.091

TABLE 4.1. *Mesh independence.*

The fluid was assumed initially at rest. The vesicle was initially a sphere with radius half of the domain. A pore was introduced by defining a sphere one twentieth the radius of the domain, centered at the pole of the vesicle. Our model does not spontaneously form a pore. The opening and closing of the pore involves the geometry of the lipid molecules at a length scale a few nanometers in diameter, much smaller than considered by classical continuum mechanical models. The exact mechanism governing the opening and closing of a pore is itself an interesting subject and is beyond the scope of this study. See, for example, [25].

4.2. A Large Vesicle with Infoldings. In the experimental practice of creating and visually recording a pore, a large vesicle tens of microns in diameter is placed in solution. These vesicles are not taut, but have small undulations while maintaining an overall spherical shape. A mechanical tension is introduced by the photoactivation of fluorescently labeled lipids which in turn leads to an excess of area. The two dimensional modulus typically associated with this unfolding is $s_0=0.045$. Furthermore, a solution with viscosity several times that of water is used to slow and make the experiments easier.

In order to compare the diffusive interface model with the classical experimental result [1], we chose a solution viscosity 30 times that of distilled water. The spatial scale λ was chosen so the the initially spherical vesicle had a radius of 20μm and the surrounding cylindrical fluid region a radius of 40μm and height 80μm. We used

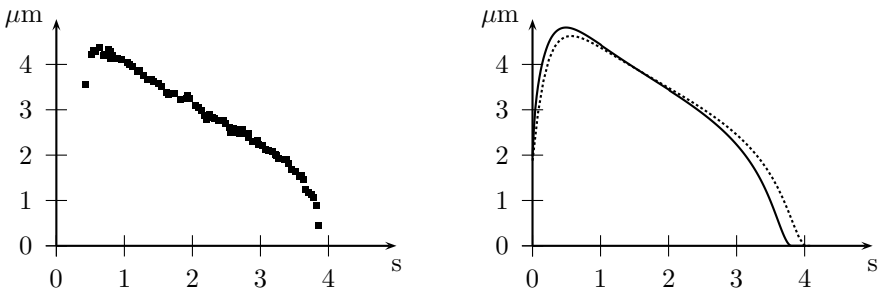

FIG. 4.2. *Experimental and simulated pore radius as a function of time. Left: microscopy data [1] for a vesicle of radius 20μm in solution with* $\eta_0 = 20cP$. *Right: the same vesicle simulated with* $s_0 = 0.045$, $w_0 = 0$, $b_0 = 20$, $j_0 = 2.5$, $\tau = 0.1$, $\eta_0 = 30$, *and* $\lambda = 40$. *Solid line:* $\gamma = \bar{\gamma} = 10^{-2}$, $m_1 = 10^3$, *and* $m_2 = 0.1$. *Dashed line:* $\gamma = \bar{\gamma} = 2 \cdot 10^{-2}$, $m_1 = 0.5 \cdot 10^3$, *and* $m_2 = 0.2$.

the realistic values $b_0 = 20$ and $j_0 = 2.5$ for the bending modulus and edge tension respectively. For this experiment, unfolding is more consequential than surface tension and so we set $w_0 = 0$.

In experiments with vesicles of this size, the life time of the pore is seconds long. Letting $\tau = 0.1$, the nondimensional coefficients in the equations were numerically comparable and the simulation results yielded a realistic time course. In Figure 4.2 we see that the pore radius as function of time compares favorably with microscopy data obtained from [1]. Figure 3.1 shows the cross section of the vesicle as well as the opening and closing of the pore. The cross sections show that the overall shape of the vesicle is spherical. At the length scale of large vesicles, the force due to mechanical tension, a spatially constant multiple of the surface normal, is orders magnitude larger than bending and edge tension. Thus, the increase in energy associated with a deviation from a spherical shape is much larger than the change in energy associated with the widening and closing of the pore. Note that in this experiment, the diffusive interface represents the apparent location of the membrane. The undulations occurring at a much smaller length scale are not resolved.

4.3. Comparison and Discussion. The simulation captures the experimentally well known, three stage form of the pore radius as function of time. Preceding the first stage, a mechanical tension is introduced by assuming the vesicle has an excess area of four percent ([11]). A small pore is introduced. The presence of the pore permits the vesicle to lose area. As seen in Figure 4.3, a rapid widening, stage one, is induced by diffusive interface force pointing away from the pore. In Figure 4.3, fluid leaks from the interior of the vesicle. In Figures 4.2 and 4.1, one sees that the maximum radius is reached and most of the energy dissipated in one tenth of the life-time of the pore.

Stage two, the linear closing, follows. The area of vesicle has assumed the resting value and length of the rim of the pore is the primary source of energy. As seen in Figures 4.3, the force pointing inward to the pore generates a contractile motion of the fluid. The rate of contraction is quite small when compared to stage one.

The pore dynamic concludes with the third, rapid closing stage. As the pore becomes smaller, the curvature increases which in turn increases the radial force due to edge tension, accelerating the pore closure. The water in the interior of the vesicle, no longer affected by Laplace pressure, is almost completely static. The pore seals due to diffusive effects of the interface. This occurs when the radius of the pore is

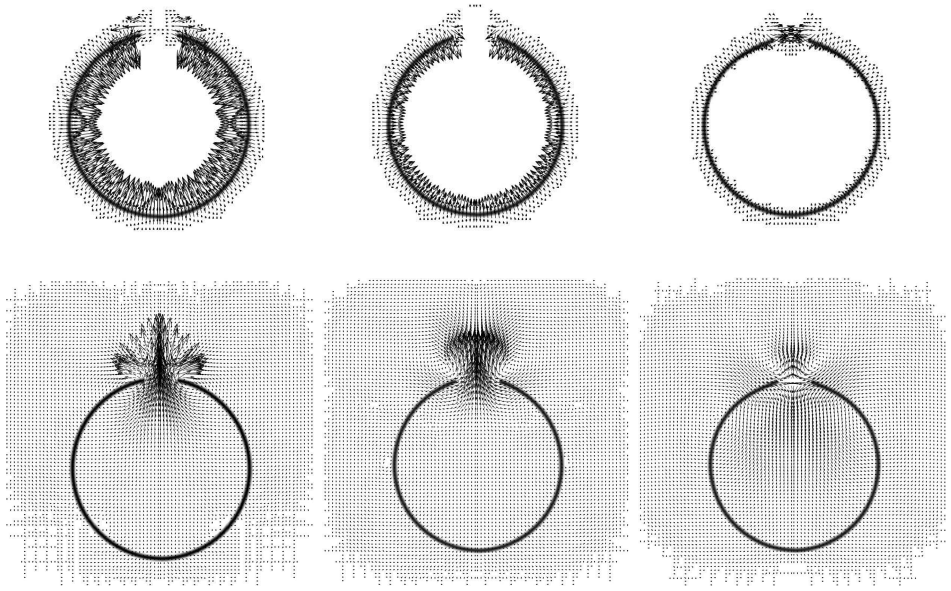

FIG. 4.3. *Top: diffusive interface forces. Initially, mechanical tension widens the pore. In the transition from stage one to stage two, mechanical tension is relaxed. In the the closing stages, edge tension closes the pore. For clarity, only one third of the arrows are plotted. Bottom: fluid velocity. Initially the flow is concentrated in the pore but quickly develops around the pore. In the closing stages, flow is more in plane with the pore.*

comparable to the diffuse interface thickness.

4.4. A Small Osmotically Stretched Vesicle. The creation of a pore by osmotic swelling is a process with considerable interest to biologists. Hemolysis, the leak out of the contents of a red blood cell, has been studied and observed by clinicians for centuries. Encouraged by the agreement of the simulation with experimental data for large vesicles, we proceed to simulate a small, osmotically swollen vesicle.

Due to dimensional scaling, small vesicles can withstand the large pressure associated with osmotic gradients by increasing their area slightly. The stretching modulus $s_0 = 60$ associated with the excess area per lipid is much larger than the one due to unfolding ([12]). The stretching tension plus the surface tension $w_0 = 1$ for submicron vesicles results in a significant Laplace pressure.

We simulated a vesicle with radius $50nm$ in a solution of distilled water. In order to resolve the time course, we chose a time scale tenths of microseconds long by setting $\tau = 10^{-8}$. The pore radius as a function of time is plotted in Figure 4.4. Qualitatively, the functional form of the graph is very similar to that of large vesicles. The pore reaches a maximum radius that is a significant fraction of the overall vesicle size. The linear closing stage is not as well defined as for large vesicles due to the nonzero surface tension w (comparison not shown.) In Figure 4.4, we have also plotted the percent outflow and sphericity of the vesicle as a function of time. The vesicle becomes slightly elliptical in stage one and is spherical after the pore closes. The total outflow of fluid

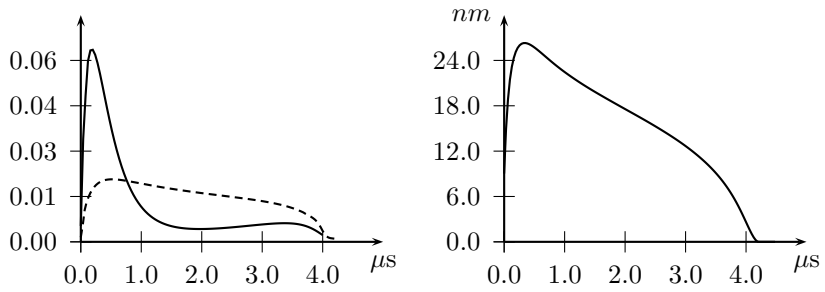

FIG. 4.4. *Simulation results for an osmotically swollen vesicle of radius 50nm in solution* $\eta_0 = 1$, *with* $s_0 = 60$, $w_0 = 1$, $b_0 = 20$, $j_0 = 2.5$, $\tau = 10^{-8}$, *and* $\lambda = 0.1$. *Left: percent leak out of vesicle volume (solid line) and sphericity (dashed line). Sphericity is defined as* $A/A_s - 1$, *where* A_s *is the area of the spherical zone with the identical volume and pore radius as the vesicle. Right: pore radius as a function of time.*

represents roughly 5% of the vesicle volume. In this case, the bilayer also assumes a shape very close to a sphere. This shows that although there is a steady efflux of water from the vesicle interior, the total outflow is small enough to not significantly alter the shape while the vesicle sheds excess area. Since mechanical tension is large, the energy dissipation mechanism dictates that the vesicle minimize surface area with respect to its fluid volume, the change of which is limited by the low Reynolds outflow though the pore.

5. Sharp Interface Limit Under suitable modeling assumptions, the energy of the open vesicle E has the sharp interface limit

$$E_0 = \int_{M_t} (bH^2 + w)\alpha_0 \, dS + s\frac{(|M_t|_{\alpha_0} - A_{\mathrm{r}})^2}{2A_{\mathrm{r}}} + j|M_t \cap \bar{M}_t| + m_2 \int_{\bar{M}_t} H^2 \, dS. \qquad (5.1)$$

Here M_t and $\bar{M}_t$ are smooth, open, orthogonal surfaces evolving with t and where $M_t \cap \bar{M}_t$ represents the rim of the pore. When ξ is large, the function $\alpha_0(x,t)$ is a positive, step wise function taking values close to 1 in the exterior of $\bar{M}_t$ and values close to 0 in the interior of $\bar{M}_t$. By $|M_t|_{\alpha_0}$ we denote that approximate area of M, namely the surface integral of α_0 over M. By $|M_t \cap \bar{M}_t|$ we denote the length of the intersection. Here H is the mean curvature of M_t or $\bar{M}_t$ and as before m_2 is a small, stabilizing parameter. Thus the diffusive interface model converges to the classical Helfrich energy of a lipid bilayer with a hole plus auxiliary terms for the surfaces used to label the position of the hole.

The modeling assumptions we make are

$$\phi(x,t) = p(d(x,t)/\epsilon) + \epsilon g_1(x,t) + \epsilon^2 g_2(x,t) + \ldots,$$
$$\bar{\phi}(x,t) = \bar{p}(\bar{d}(x,t)/\epsilon) + \epsilon \bar{g}_1(x,t) + \epsilon^2 \bar{g}_2(x,t) + \ldots,$$

where $d(x,t)$ and $\bar{d}(x,t)$ are the signed distance function to smooth, closed, transverse surfaces M_t and $\bar{M}_t$ in D respectively. The surfaces M_t and $\bar{M}_t$ are the boundary of respective set of points were ϕ and $\bar{\phi}$ are positive in the limit $\epsilon = 0$. The functions p and $\bar{p}$ describe the profile of the labeling functions in this limit and $g_1, g_2, \bar{g}_1$, and $\bar{g}_2$ are smooth functions independent of ϵ. We are assuming that E is bounded by a constant independently of ϵ and the other modeling parameters. This assumption is reasonable since the energy is known (by the dissipation relation (3.8)) to be nonincreasing and initial data for the labeling functions may chosen for which this bound holds.

In [5] and [6], a related problem was analyzed for a single diffusive interface approximation of the Willmore–mean curvature squared–energy with surface area and volume constraints. With the above assumptions, Theorems 2.1 and 2.2 of [5] imply that that $p(r)=\bar{p}(r)=\tanh(r/\sqrt{2})$ and $g_1\equiv\bar{g}_1\equiv 0$. Summarizing the argument, the energy E is expanded in powers of ϵ. Collecting the lowest order terms, the energy remains bounded provided p and $\bar{p}$ are solutions to the ordinary differential equation $p''-p(p^2-1)$. The boundary conditions (3.6) then imply that p and $\bar{p}$ are profiles given by the hyperbolic tangent function. The remaining terms in the expansion of E involves the square norm of g_1 and $\bar{g}_1$. These terms are bounded independently of ϵ provided g_1 and $\bar{g}_1$ are identically zero. By making only slight modifications to account for the term α appearing in the integrand of W and A, we can apply Theorem 4.1 of [5] to recover the sharp interface limit for the surface integrals appearing in (5.1).

It remains to show that the diffusive interface approximation L converges to the length of the rim of the pore $|M_t\cap\bar{M}_t|$. The constraint functional P was introduced in [26] to ensure that the diffusive interfaces are effectively orthogonal. We use expansion and the boundedness of P to conclude that M_t and $\bar{M}_t$ are orthogonal. Note that gradient of the distance functions are a multiple of the unit normals n and $\bar{n}$ of M_t and $\bar{M}_t$ respectively. Using the continuity of the functions ∇d and $\nabla\bar{d}$ in a neighborhood of the curve $M_t\cap\bar{M}_t$, the first term in the expansion of P in ϵ is bounded below by

$$c\epsilon^{-4}\int_{M_t\cap\bar{M}_t}(n\cdot\bar{n})^2\,dl$$

for some constant c independent of ϵ. Since this quantity is bounded independent of ϵ, we infer that M_t and $\bar{M}_t$ are orthogonal. Using Lemma 2.2 of [5], the remaining terms in the expansion of P vanish with ϵ. Thus, the boundedness of P and the asymptotic assumptions imply that $\lim_{\epsilon\to 0}P=0$.

The orthogonality of sharp interface limits is now sufficient to imply that the approximation L actually converges to the length of the rim of the pore. This is achieved by first assuming that $M_t\cap\bar{M}_t$ is piecewise linear and passing to the limit $\epsilon=0$. The general case follows by approximation and the standard diagonal argument. Consider the rectangular cylinder $Q=\{(x_1,x_2,x_3):0<x_3<l,-\sqrt{\epsilon}<x_1,x_2<\sqrt{\epsilon}\}$. Assume, without loss of generality, that $M_t\cap\bar{M}_t\cap Q$ lies in the x_3-axis and n and $\bar{n}$ are parallel with the coordinate directions. This assumption is possible since the interfaces are orthogonal. As ϵ approaches 0, the signed distance functions d and $\bar{d}$ are uniformly approximated by the coordinate functions x_1 and x_2. Using the identities $F(p)=(p^2-1)^2=(p')^2/2$ and $\lim_{\epsilon\to 0}\int_{-\sqrt{\epsilon}}^{\sqrt{\epsilon}}\frac{1}{\epsilon}q'(s/\epsilon)^2\,ds=\frac{2\sqrt{2}}{3}$, we evaluate the limit

$$\lim_{\epsilon\to 0}\int_Q\left(\frac{\epsilon}{2}|\nabla\phi|^2+\frac{1}{\epsilon}F(\phi)\right)\left(\frac{\epsilon}{2}|\nabla\bar{\phi}|^2+\frac{1}{\epsilon}F(\bar{\phi})\right)dx=\frac{8}{9}l=\frac{8}{9}|M_t\cap\bar{M}_t\cap Q|.$$

To calculate that entire length, we cover $M_t\cap\bar{M}_t$ by a union of cylinders, noting that the integrand vanishes exponentially on the exterior of the cover, and the contribution from the overlap vanishes in the limit $\epsilon=0$. This show that $\lim_{\epsilon\to 0}L=|M_t\cap\bar{M}_t|$. This concludes the demonstration of the sharp interface limit (5.1).

6. Conclusion. The diffusive interface model captures the dynamic shape of an open vesicle where the membrane and water is impelled by surface and line forces. The numerical method is stable, encompasses a wide range of length and time scales through scaling parameters, and is capable of producing realistic time courses of vesicles and their flow fields below the experimentally observable limits. The simulation

results for large vesicles are in good quantitive agreement with classical experiments. The model converts large amounts of energy stored in mechanical stretching into fluid motion, edge energy and heat. The simulations indicate that the overall shape of the vesicle remains sphere-like throughout the time course.

The model was unable to produce a pore spontaneously. An initial, small pore was assumed and sealing is an artifact of the diffusive interface representation. Future work will study functionals for which spontaneous pore formation is an energy minimizing path.

Acknowledgement. It is a pleasure to thank Chun Liu for introducing us to each other, and initiating this collaboration and application. We thank Gary Leaf for making available computing resources at Argonne National Lab. RR was supported by a Fordham 1st Year Research Grant and FSC was supported by NIH GM 066837.

REFERENCES

[1] Brochard-Wyart, de Gennes, and Sandre, *Transient pores in stretched vesicles: role of leakout*, Physica A 278 (2000)
[2] Caginalp and Chen, *Convergence of the phase field model to its sharp interface limits*. European Journal of Applied Mathematics 9 (1998).
[3] Du, Liu, and Wang, *A phase field approach in the numerical study of the elastic bending energy for vesicle membranes*. Journal of Computational Physics 198 (2004).
[4] Du, Li, and Liu, *Analysis of a Phase Field Navier-Stokes Vesicle-Fluid Interaction Model*. DCDS B, 8 (2007).
[5] Du, Liu, Ryham, and Wang, *A phase field formulation of the Willmore problem*. Nonlinearity 18 (2005).
[6] Du, Liu, Ryham, and Wang, *Energetic variational approaches in modeling vesicle and fluid interactions*. Physica D 238, 9-10 (2009).
[7] Evans, *Partial Differential Equations*. AMS Graduate Studies in Mathematics (1991).
[8] Lawrence Evans and Halil Soner, *Phase transitions and generalized motion by mean curvature*. Communications on Pure and Applied Mathematics, XLV (1992).
[9] Glowinski, Ciarlet and Lions, *Handbook of Numerical Analysis: Numerical Methods for Fluids*. Volume 9, Part 3 (2003).
[10] Helfrich, *Elastic properties of lipid bilayers-theory and possible experiments*. Zeitschrift für Naturforschung C, 28 (1973).
[11] Karatekin, Sandre, Guitouni, Borghi, Puech and Brochard-Wyart, *Cascades of Transient Pores in Giant Vesicles: Line Tension and Transport*. Biophysical Journal 84 (2003).
[12] Kuzmin, Akimov, Chizmadzhev, Zimmerberg and Cohen, *Line Tension and Interaction Energies of Membrane Rafts Calculated from Lipid Splay and Tilt*. Biophysical Journal 88 (2005).
[13] Levin and Idiart, *Pore dynamics of osmotically stressed vesicle*. Physica A 331 (2004).
[14] Lowengrub, Xu and Voigt, *Surface Phase Separation and Flow in a Simple Model of Multicomponent*. Fluid Dynamics and Materials Processing, **3**, no. 1 (2007).
[15] Modica, *The gradient theory of phase transitions and the minimal interface criterion*. Archive for Rational Mechanics and Analysis, Volume 98, Number 2 (1987).
[16] Moser, *A higher order asymptotic problem related to phase transitions*. SIAM J. Math. Anal. 37, (2005).
[17] Moroz and Nelson, *Dynamically stabilized pores in bilayer membranes*. Biophysical Journal Vol. 72 (1997).
[18] Puech and Brochard-Wyart, *Membrane tensiometer for heavy giant vesicles*. Eur. Phys. J. E 15, (2004).
[19] Portet and Dimova, *A New Method for Measuring Edge Tension and Stability of Lipid Bilayers: Effect of Membrane Composition*. Biophysical Journal 99 (2010).
[20] Röger and Schätzle, *On a Modified Conjecture of DeGiorgi*. Mathematische Zeitschrift 245, no. 4 (2006).
[21] Sohn, Tseng, Li, Voigt, and Lowengrub, *Dynamics of multicomponent vesicles in a viscous fluid*. Journal of Computational Physics, 229 (2010).

[22] Veerapaneni, Young, Vlahovska and Bławzdziewicz, *Dynamics of a Compound Vesicle in Shear Flow*. Physical Review Letters 106 (2011).
[23] Vlahovska, Young, Danker and Misbah, *On the complex dynamics of a red blood cell in simple shear flow*. To appear in Journal of Fluid Mechanics (2011).
[24] J. D. Van der Waals, *Thermodynamic theory of capillarity assuming continuous change of density*. Natuurk. Verb. Kon. Akad. Amsterdam 1 (1892).
[25] Wohlert, den Otter, Edholm and Briels, *Free energy of a trans-membrane pore calculated from atomistic molecular dynamics simulations*. Journal of Chemical Phyiscs 124 (2006).
[26] Wang and Du, *Modeling and simulations of multi-component lipid membranes and open membranes via diffuse interface approaches*. J. Math. Biol. 56 (2008).